

Introduction

Dose calculation errors near metal implants are caused by limitations of the dose calculation algorithm in modeling tissue/metal interface effects as well as density assignment errors caused by imaging artifacts. The purpose of this study was to investigate two strategies for reducing dose calculation errors near metal implants: implementation of metal-based energy deposition kernels in the convolution/superposition (C/S) dose calculation method and use of metal artifact reduction methods for computed tomography (CT) imaging.

Three commercial CT metal artifact reduction methods were investigated. Philips Healthcare's O-MAR, GE Healthcare's monochromatic gemstone spectral imaging (GSI), and GSI imaging with metal artifact reduction software applied (MARs). The O-MAR algorithm is an iterative projection modification solution for polyenergetic CT imaging,¹ while GSI imaging uses dual-energy CT data. GSI monochromatic images depict how an object would look if it were imaged using a monoenergetic X-ray source and have reduced beam hardening artifacts in comparison to conventional polyenergetic images.² The MARs algorithm is designed to be used with GSI imaging to further reduce artifacts caused by photon starvation.³

In addition to imaging artifacts, dose calculation errors also result from the limited ability of modern dose calculation algorithms to model radiation transport in and near metal implants. For the C/S algorithm, the density scaling approximation is used for heterogeneous dose calculations, i.e., water-based energy deposition kernels are simply scaled in dimension based on the local density encountered. This density scaling of water kernels is only a good approximation for materials with the same atomic composition as water and thus may be inadequate to describe the physical interactions and scatter occurring in metal implants.⁴ In this study, metal-based kernels were implemented into commercial collapsed cone C/S algorithm to address this limitation of the dose calculation algorithm.

Metal artifact reduction (MAR) study

Methods: Both error-reduction strategies were evaluated using a simple slab phantom that can accommodate one of two metal inserts, either a 2 cm thick titanium insert or a 4mm thick Cerrobend insert. The dose upstream and downstream of the metal was measured for a single incident 6MV photon beam using EBT2 radiochromic film (Gafchromic, Ashland, Wayne, NJ). The phantom was imaged using uncorrected, baseline CT imaging (120kVp) and metal artifact reduction methods (O-MAR, GSI, and MARs). Dose calculations were performed using Mobius3D v1.3.1 (Mobius Medical Systems, LP, Houston, TX) using two different CT calibration curves (for polyenergetic 120kVp imaging and monochromatic 140keV imaging).

MAR study continued

Results: Figure 1 and Table 1 show the results of our metal artifact reduction study. In the downstream region, systematic errors were observed for both metals for dose calculations performed with uncorrected CT images (>20% for titanium and >50% for Cerrobend). For titanium, O-MAR was able to decrease errors, while GSI imaging had very little dosimetric impact. MARs created an artificial low-density pocket inside the titanium insert (Figure 2b) and substantially increased errors in the downstream region in comparison to uncorrected CT imaging. In contrast, MARs successfully reduced artifacts and more accurately represented the thickness of the Cerrobend implant (Figure 2e and 2f) and was the only method that reduced calculation errors for Cerrobend.

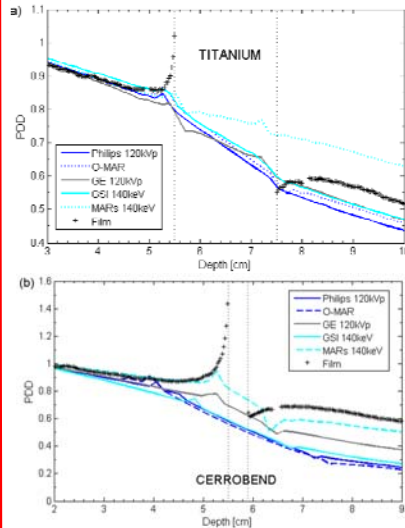


Figure 1: Percent depth dose (PDD) curves calculated for (a) titanium and (b) Cerrobend using baseline imaging techniques (Philips 120kVp and GE 120kVp) and metal artifact reduction methods (O-MAR, GSI 140keV, and MARs 140keV). The dose measured with film is also shown.

Table 1: The mean absolute % error between calculated and film-measured dose. Dose calculations were performed using various baseline imaging methods and metal artifact reduction methods. The upstream region extends from d_{max} to the proximal interface, while the downstream region extends from the distal interface to 5 cm beyond the metal implant.

Imaging technique	Titanium		Cerrobend	
	Upstream	Downstream	Upstream	Downstream
Philips 120kVp	1.4	15	10.1	53.7
O-MAR	1.1	11.1	10.3	56.4
GE 120kVp	1.9	9	7.3	33
GSI 140keV	1.9	8.7	12	49.6
MARs 140keV	1.4	21.8	2.5	14.7

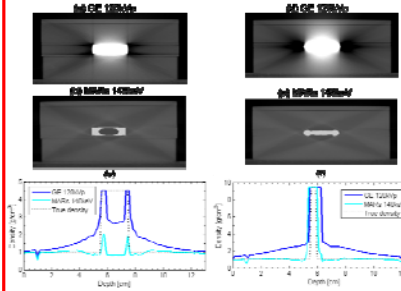


Figure 2: Panels (a) and (d) show 120kVp images of the titanium and Cerrobend phantom configurations, respectively, while panels (b) and (e) show the same image slice using MARs 140keV imaging, illustrating the artificial introduction of a low-density pocket within the titanium insert in (b). Panels (c) and (f) show the density assignment along the central axis using both imaging methods, along with the true density

Metal kernel study

Methods: Metal kernel dose calculations were performed for an "ideal" phantom geometry (with density overrides performed for the metal insert and the streak artifacts) to investigate the impact of metal kernels without the confounding effects of imaging artifacts. Dose calculations were performed with the Mobius3D algorithm, using a metal density threshold. For voxels with an assigned density greater than the threshold value, metal kernels were used to describe the energy deposition for energy released from those voxels. For voxels with assigned density less than the metal threshold, water kernels were used. Dose calculations were also performed with Pinnacle CCC and Eclipse AAA for comparison.

Results: Table 2 and Figure 3 show the results from our metal kernel dose calculations. Metal kernels were found to better model the backscatter dose enhancement at the proximal interface and generally improved accuracy upstream of the metal. However, metal kernels slightly worsened accuracy directly downstream of the metal. The accuracy of metal kernel dose calculations was somewhat dependent on dose grid size, with small calculation voxels tending to result in better accuracy.

Table 2: The mean absolute % error between calculated and film-measured dose for dose calculations performed with Mobius3D with and without metal kernels (MK). The % error is reported for the region 1 cm upstream of the proximal interface and the region 1 cm downstream of the distal interface.

Metal	Dose grid size (mm)	% Error (no MK / MK)	
		Upstream 1 cm	Downstream 1 cm
Titanium	1.25	1.5 / 1.2	2.4 / 3.7
	1.5	1.4 / 1.8	2.2 / 6.1
	3	1.7 / 1.8	4.5 / 7.9
Cerrobend	1.25	9.2 / 8.2	2.6 / 2.0
	1.5	9.0 / 7.5	2.8 / 6.6
	3	9.4 / 8.2	3.7 / 4.3

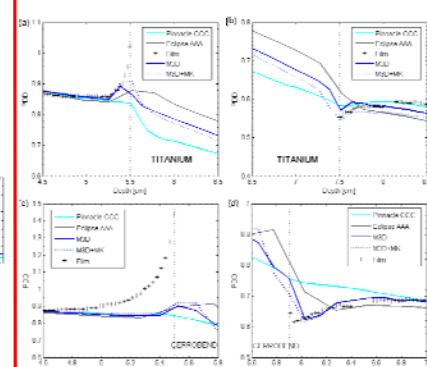


Figure 3: Percent depth dose (PDD) curves for dose calculations performed using Mobius3D with ("M3D+MK") and without ("M3D") metal kernels for (a) the proximal interface of the titanium insert, (b) the distal interface for titanium, (c) the proximal interface for Cerrobend, and (d) the distal interface for Cerrobend. The dose measured with film is also shown. Dose calculations for M3D were performed for a uniform 1.25-mm dose grid.

Conclusions

- The CT artifact reduction methods were generally more successful for titanium than high Z Cerrobend
- Accurate representation of the size of metal implants in CT images is an important factor for accurate dose calculations (more so than reducing streak artifacts)
- The MARs algorithm can result in metal distortion, sometimes improving accuracy (Cerrobend) but sometime substantially worsening accuracy (titanium). Thus MARs should be used with caution for treatment planning.
- Metal kernels improved accuracy at the upstream interface but decreased accuracy at the downstream interface
- Metal kernel dose calculations were somewhat dependent on dose grid size, with finer resolution yielding better accuracy.

References

- Philips White Paper, "Metal artifact reduction for orthopedic implants (O-MAR)." Philips Healthcare 2012.
- L. Yu, S. Leng and C. H. McCollough, "Dual-energy CT-based monochromatic imaging," AJR Am. J. Roentgenol. **199**, S9-S15 (2012).
- S. Y. H. Lee, K. K. Park, H. T. Song, S. Kim and J. S. Suh, "Metal artefact reduction in gemstone spectral imaging dual-energy CT with and without metal artefact reduction software," Eur. Radiol. **22**, 1331-1340 (2012).
- J. Y. Huang, D. Eklund, N. L. Childress, R. M. Howell, D. Mirkovic, D. S. Followill and S. F. Kry, "Investigation of various energy deposition kernel refinements for the convolution/superposition method," Med. Phys. **40**, 121721 (2013).

Support

The investigation was supported by PHS grant CA10953 and CA081647 awarded by the NCI, DHHS.

Contact: jjanshu@gmail.com